Contents lists available at ScienceDirect

Journal of Organometallic Chemistry

journal homepage: www.elsevier.com

Solvent effects on the photophysical properties of $Bu_4N[(4,4'\text{-bpy})Re(CO)_3(bpy\text{-}5,5'\text{-diCOO})]$ complex. A combined experimental and computational study

Hector H. Martinez Saavedra,[a] Fabricio Ragone,[a] Carlos A. Franca,[b] Gustavo T. Ruiz,[a] Pedro M. David Gara,[c, **] Ezequiel Wolcan [a, *]

[a] *Instituto de Investigaciones Fisicoquímicas Teóricas y Aplicadas (INIFTA, FCE-UNLP, CONICET), Diag. 113 y 64, C.C. 16 Sucursal 4, B1906ZAA, La Plata, Argentina*
[b] *Centro de Química Inorgánica (CEQUINOR), 47 y 115, C.C. 962, 1900, La Plata, Argentina*
[c] *Centro de Investigaciones Ópticas (CIOp, CONICET-CIC) and UNLP, C.C. 3, 1897, La Plata, Argentina*

ARTICLE INFO

Article history:
Received 6 April 2016
Received in revised form 10 May 2016
Accepted 12 May 2016
Available online xxx

Keywords:
Re(I) tricarbonyl complex
Solvent effects
TD-DFT
Photophysics
Triplet energy calculation

ABSTRACT

The photophysical properties of the complex $Bu_4N[(4,4'\text{-bpy})Re(CO)_3(bpy\text{-}5,5'\text{-diCOO})]$ were studied in protic and aprotic media with the aid of steady-state and time-resolved techniques and TD-DFT calculations. The absorption spectrum as well as the steady state and time resolved luminescence of the Re(I) complex display a marked solvent effect. The highest and lowest energy absorption bands experience a bathochromic shift as the polarity of the solvent decreases. In addition, the lowest energy band broadens. Two luminescence bands were observed around 430 and 600 nm in protic organic solvents like alcohols. The high energy emission is observed solely in aqueous solutions, while in aprotic solvents only the low energy luminescence is detected. TD-DFT calculations allowed us to identify the main electronic transitions in the low energy region as $^1MLLCT_{Re(CO)_3 \rightarrow 4,4'\text{-bpy}}$ and $^1MLLCT_{Re(CO)_3 \rightarrow bpy\text{-}5,5'\text{-diCOO}}$. The simulated absorption spectra of the Re(I) complex in H_2O, protic (EtOH, MeOH) and aprotic ($CHCl_3$, CH_2Cl_2, CH_3CN) organic solvents follow the experimental absorption spectra with reasonable accuracy both in position and relative intensities. The magnitude of the calculated dipole moment (μ) increases with the dielectric constant of the solvent (ε_r). Besides, the energy of $^1MLLCT_{Re(CO)_3 \rightarrow 4,4'\text{-bpy}}$ also increases with ε_r. However, the energy of the $^1MLLCT_{Re(CO)_3 \rightarrow bpy\text{-}5,5'\text{-diCOO}}$ transition is rather insensitive to ε_r. This disparity is attributed to the fact that the $^1MLLCT_{Re(CO)_3 \rightarrow 4,4'\text{-bpy}}$ transition is nearly parallel to the orientation of μ while the $^1MLLCT_{Re(CO)_3 \rightarrow bpy\text{-}5,5'\text{-diCOO}}$ transition is almost perpendicular to it. Unrestricted TDFT calculations were successfully applied to the triplet species. It is observed that in the triplet state the Re—N distances are shortened while Re—C distances are elongated relative to the ground state. The calculated emission energy by TD-DFT and/or Δ(SCF) methods was compared to the experimental emission maximum in chloroform. All the experimental results as well as the theoretical calculations indicate that solvent effects on the steady state and time resolved luminescence of the Re(I) complex can be accounted by the coexistence of $^3MLLCT_{Re(CO)_3 \rightarrow 4,4'\text{-bpy}}$, $^3MLLCT_{Re(CO)_3 \rightarrow bpy\text{-}5,5'\text{-diCOO}}$ and ^1IL excited states.

© 2016 Published by Elsevier Ltd.

1. Introduction

The nature of the axial X ligand in *fac*-$ReX(CO)_3$(α-diimine) complexes determines the fact that these compounds may or may not be strong luminophores, either in fluid solutions or at low-temperature glasses. The accessible excited states, $Re(CO)_3$ to αligand charge transfer (LLCT), and/or intraligand (IL) excited states, are generally involved with their observed luminescence at room temperature. Due to the fact that they are thermally and photo-chemically stable as well as rich in their excited-state behavior and redox chemistry these complexes have been used in broad research areas such as electron transfer studies [1], solar energy conversion [2–4], catalysis [5], as luminescent sensors [6–8], and as labeling reagents and non-covalent probes for biomolecules and ions [9–11]. For instance, biochemical applications based on the formation of adducts between these rhenium complexes and biomolecules like DNA have emerged [12,13]. A major drawback, however, relies on their limited solubility in aqueous media. In fact, most of the *fac*-$ReX(CO)_3$(α-diimine) complexes which annually appear on the literature reports are exclusively soluble in organic solvents while only a few of them can be managed in aqueous solutions at physiological pHs [14–21]. In previous work we have synthesized and characterized a water soluble *fac*-$ReX(CO)_3$(α-diimine) complex coordinating the ligands 2,2′-bipyridine-5,5′- dicarboxylate (bpy-5,5′-diCOO) and 4,4′-bipyridine (4,4′-bpy) [22]. In the $Bu_4N[(4,4'\text{-bpy})Re(CO)_3(bpy\text{-}5,5'\text{-diCOO})]$ complex structure the two negative charges of the carboxylate groups are balanced by the positive charges of the Re(I) center and that of a tetrabutyl ammonium cation (See Scheme 1). The pH dependent UV-vis spectroscopy of the Re(I) complex was compared with TD-DFT calculations on the different acid-base species existing in aqueous solutions and the nature of the responsible electronic transitions was established [22]. A switch between a $MLLCT_{Re(CO)_3 \rightarrow bpy\text{-}5,5'\text{-diCOO}}$ to a $MLLCT_{Re(CO)_3 \rightarrow 4,4'\text{-bpy}}$ character of the lowest energy excited state occurred when the 4,4′-bpy ligand was protonated explaining the overall spectral changes in the 350–500 nm range after protonation of

* Corresponding author.
** Corresponding author.
Email addresses: pedrodg@ciop.unlp.edu.ar (P.M. David Gara); ewolcan@inifta.unlp.edu.ar (E. Wolcan)

http://dx.doi.org/10.1016/j.jorganchem.2016.05.012

UNCORRECTED PROOF

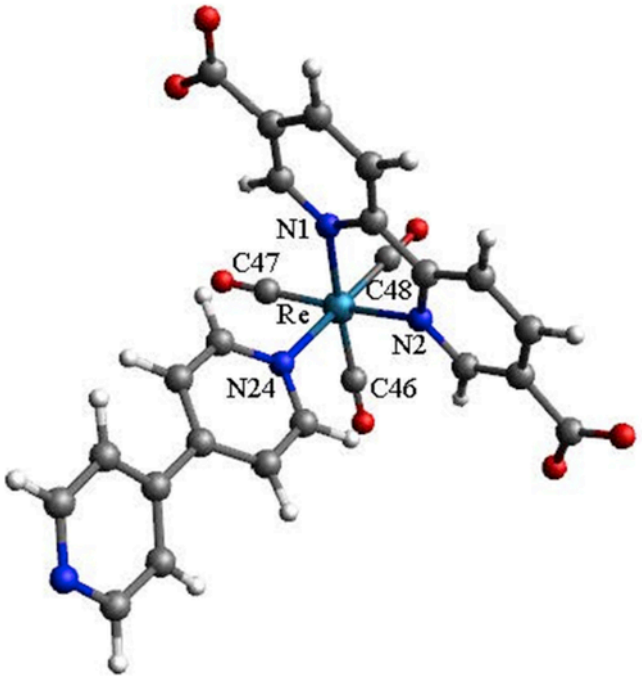

Scheme 1. Optimized structure of $Bu_4N[(4,4'\text{-bpy})Re(CO)_3(bpy\text{-}5,5'\text{-diCOO})]$ complex with atoms numbering.

the Re(I) complex [22]. With the aim of further deepening the understanding of the role of the different excited states on the electronic structure of the complex, in this paper we continue with the study of the photophysical properties of $Bu_4N[(4,4'\text{-bpy})Re(CO)_3(bpy\text{-}5,5'\text{-diCOO})]$. For this purpose, laser induced optoacoustic spectroscopy (LIOAS), steady-state and time-resolved luminescence techniques as well as time-dependent density functional theory (TD-DFT) calculations were performed in both protic and aprotic media. The luminescence behavior of the Re(I) complex showed a strong solvent dependence. When the spectrum was taken in water the emission occurred peaking at $\lambda_{max} = 435$ nm. In the aprotic solvents the maximum of the luminescence spectrum occurred at 604, 595 and 570 nm for CH_3CN, CH_2Cl_2 and $CHCl_3$, respectively. In MeOH and EtOH, however, two peaks were observed; one at 425 and the other around 600 nm. Depending on the solvent, two or three exponential functions were needed to achieve a satisfactory fit of the time resolved luminescence decays. The presence of O_2 in the solutions quenched both the steady state and time resolved luminescence of the Re(I) complex in all the solvents. The calculated dipole moment, μ, increased monotonically with the solvent dielectric constant, ε_r. While the calculated energy of the $MLLCT_{Re(CO)_3 \rightarrow 4,4'\text{-bpy}}$ transition increased with the increase of μ, the calculated energy of the $MLLCT_{Re(CO)_3 \rightarrow bpy\text{-}5,5'\text{-diCOO}}$ transition remained essentially constant. In addition, unrestricted TD-DFT calculations on the triplet state were performed. These calculations showed that the S_0-T_n transition should be viewed as a delocalized MLLCT transition where the electronic charge is transferred from $Re(CO)_3$ moiety to both 4,4′-bpy and bpy-5,5′-diCOO ligands. All the experimental results as well as the theoretical calculations indicate that solvent effects on the steady state and time resolved luminescence of the $Bu_4N[(4,4'\text{-bpy})Re(CO)_3(bpy\text{-}5,5'\text{-diCOO})]$ complex can be accounted by the coexistence of $^3MLLCT_{Re(CO)_3 \rightarrow 4,4'\text{-bpy}}$, $^3MLLCT_{Re(CO)_3 \rightarrow bpy\text{-}5,5'\text{-diCOO}}$ and ^1IL excited states.

2. Experimental

2.1. Materials

The complex $Bu_4N[(4,4'\text{-bpy})Re(CO)_3(bpy\text{-}5,5'\text{-diCOO})]$ was available from previous work [22]. Spectrograde and HPLC grade acetonitrile, chloroform and methanol (MeOH) from J.T. Baker, and ethanol (EtOH) and dichloromethane from Sigma Aldrich were used without further purification. 2-Hydroxybenzophenone (2-HBP), phenalenone, D_2O and NaOH were purchased from Sigma Aldrich at the highest purity available and were used as received. Deionized water (>18 MΩ cm^{-1}, <20 ppb of organic carbon) was obtained with a Millipore system.

2.2. Photophysical measurements

The UV-visible absorption spectra were obtained with a Shimadzu UV-1800 spectrophotometer. Steady-state fluorescence measurements were performed using a computer-interfaced Near-IR Fluorolog-3 Research Spectrofluorometer, and were corrected for differences in spectral response and light scattering. Both measurements were performed at room temperature (*ca.* 25 °C) in quartz cells (1 cm path length). Solutions were deaerated with O_2-free nitrogen in a gas-tight apparatus before recording the spectra.

Emission quantum yields, Φ_{em}, were calculated with eq. (1), by using solutions of a reference compound (Rhodamine B in ethanol, $\Phi_{ref} = 0.69$) [23]:

$$\Phi_{em} = \left(\frac{A_{ref}}{A_s}\right)\left(\frac{I_s}{I_{ref}}\right)\left(\frac{n_s}{n_{ref}}\right)^2 \Phi_{ref} \quad (1)$$

where n_s and n_{ref} are the refractive indexes of the solutions containing the sample and the reference compound, respectively, A is the absorbance of the sample or reference at the excitation wavelength (A_s and $A_{ref} < 0.1$), and I is the integral of the emission spectrum and was used as a relative measure of the respective intensities of the luminescence. Lifetime measurements were performed at room temperature using the Time-correlated Single-Photon Counting (TCSPC) unit of the Fluorolog-3 with 341 nm NanoLED excitation source.

Photoacoustic measurements were performed by using a set-up already described [24]. Basically, a Q-Switched Nd:YAG laser (Surelite II, Continuum, 7 ns FWHM) operating at 355 nm was used as excitation source. The fluence of the laser pulses was varied using a neutral density filter, and the energy values were measured with a pyroelectric energy meter (Laser Precision Corp. RJ7620 and RJP-735). The laser beam was shaped by a 1 mm diameter pinhole in front of the cuvette, so that the resolution time in our experimental set-up, τ_R, was ca. 800 ns [25]. The detecting system consisted of a 4 mm thick x 4 mm in diameter home-made ceramic piezoelectric transducer (PZT), pressed against a cuvette side wall parallel to the laser beam direction. The detected acoustic signals were amplified, digitized by a digital oscilloscope (TDS 3032, Tektronix), and stored in a personal computer for further treatment of the data. New Coccine or 2-HBP were used as calorimetric reference (CR) compounds in the buffer and in CH_3CN solutions, respectively [26,27]. A at λ_{exc} for the CR and the sample were matched within 5%. Under the same experimental conditions for the sample and the CR, the signals generated by 64 laser shots were averaged to obtain a better signal to noise ratio. The absorption spectrum of the solution was checked before and after

UNCORRECTED PROOF

each set of laser shots, in order to detect possible sample degradation. Solutions were deaerated by bubbling N_2 or O_2 for 15 min before each experimental run. Given an excited species with a lifetime τ, if $\tau \leq {}^1/_5\tau_R$ then this species releases its heat content as prompt heat. On the other hand, when $\tau > 5\tau_R$ the excited species functions as heat storage within the time resolution of the LIOAS experiment.

The peak to peak amplitude of the first optoacoustic signal (H) is related to the fraction of the excitation laser fluence (F) absorbed by the sample by Eq. (2) [25], which was used for the handling of the LIOAS signals

$$H = K\,\alpha\,F\,(1-10^{-A}) \tag{2}$$

where the experimental constant K contains the thermo-elastic parameters of the solution as well as instrumental factors. A and α represent, respectively, the absorbance of the sample at the excitation wavelength and the fraction of the energy released to the medium as prompt heat.

The efficiency of the Re(I) complex toward singlet oxygen sensitization was assessed by the direct measurement of the $^1O_2$ ($^1\Delta_g$) near-infrared luminescence. After the irradiation of aerated solutions of the complex the generation of $^1O_2$ ($^1\Delta_g$) was evidenced by the appearance of the characteristic $^1O_2$ ($^1\Delta_g$) $\rightarrow$ $^3O_2$ phosphorescence at 1270 nm. Time resolved phosphorescence detection was used for singlet oxygen detection. The near IR luminescence of $^1O_2$ ($^1\Delta_g$) was observed at 90° geometry through a 5 mm thick anti reflective coated silicon metal filter with a wavelength pass > 1.1 μm and an interference filter at 1.27 μm by means of a pre-amplified (low impedance) Ge-photodiode (Applied Detector Corporation, time resolution 1 μs). Simple exponential analysis of the emission decay was performed with the exclusion of the initial part of the signal. The quantum yield of $^1O_2$ ($^1\Delta_g$) formation, Φ_Δ, was determined by measuring its phosphorescence intensity using an optically matched solution of phenalenone ($\Phi_\Delta = 0.98$) [28] as a reference sensitizer.

2.3. Computational details

The electronic structure of the rhenium complex was studied by performing Density Functional Theory [29–31] (DFT) and Time Dependent DFT [32–34] (TD-DFT) calculations using Gussian 09 software [35]. The ground state structure of the complex was optimized by DFT calculations using B3LYP functional and LanL2DZ basis set. Vibrational frequencies were computed at the same level of theory to confirm that these structures were minima on the energy surfaces. Solvents effects ($CHCl_3$, CH_2Cl_2, CH_3CN, EtOH, MeOH and H_2O) on the optimization of the ground state structure were taken into account by means of the Polarizable Continuum Model (PCM) [36–38]. At the optimized ground state geometries, a set of 200 vertical excitations were computed with either the B3LYP, M06 and PBE0 hybrid functional in the six solvents mentioned above. LanL2DZ basis set was used for all the atoms in TD-DFT calculations with the B3-LYP and M06 functional. TD-DFT calculations with the PBE0 functional were performed using the 6-311++G(d,p) basis set for C, N, O and H atoms while LanL2TZ(f) [39,40] (triple zeta basis set designed for an ECP plus f polarization) was used for Re atom. Percentage compositions of different molecular fragments to molecular orbitals (MOs) from output files generated from Gaussian 09 were calculated using the AOMix program [41]. Absorption spectra were simulated with Gaussian distributions with a full-width at half-maximum (fwhm) set to 3000 cm^{-1} with the aid of GaussSum 2.2.5 program.

For characterization of the electronic transitions as partial charge transfer (CT) transitions, the following definition of the CT character can be used, eq. (3) [42]:

$$CT_I\,(\%) = 100\,(P_g(\mathrm{M}) - P_I\,(\mathrm{M})) \tag{3}$$

where P_g(M) and P_I(M) are electronic densities on the metal in the electronic ground state and the I-th excited state, respectively. Positive CT_I(M) values correspond to MLCT transitions, negative CT_I(M) values correspond to LMCT transitions [42].

We can rewrite this definition by using the atomic orbital contribution to a particular MO. Therefore, the CT character for a H−n → L + m excitation is, eq. (4):

$$CT(\%) = \%(Re)_{\mathrm{H-n}} - \%(Re)_{\mathrm{L+m}} \tag{4}$$

If the excited state is formed by more than one one-electron excitation, then the metal CT character of this excited state is expressed in eq. (5) as a sum of CT characters of each participating excitation, $i \rightarrow j$ [42].

$$\mathrm{CT_I}(\%) = \sum_i \left[C_I(i \rightarrow j)\right]^2 \left[\%(M)_i - \%(M)_j\right] \tag{5}$$

where C_I(i→j) are the appropriate coefficients of the I-th transition giving the percentage contribution of a configuration to the resulting excited state TD-DFT wave function.

3. Results and discussion

3.1. Absorption spectroscopy

The UV-vis spectrum of the Re(I) complex in aqueous solutions at pH = 7 consists of one intense absorption band centered at λ_{max} = 252 nm, a set of three intense bands centered at λ_{max} = 293, 317 and 332 nm and a less intense broad absorption spanning between 350 and 450 nm. In organic solvents, relative to aqueous solutions, the band centered in H_2O at λ_{max} = 252 nm experiences a bathochromic shift as the polarity of the solvent is decreased. The complex set of bands centered at λ_{max} = 293, 317 and 332 nm in H_2O tend to crowd together as the solvent polarity is decreased and finally in CH_2Cl_2 only a band centered at λ_{max} = 309 nm is observed. In addition, the low energy and less intense absorption band broadens and experiences a bathochromic shift upon reducing solvent polarity, see Fig. 1.

Previous TD-DFT studies [22] on the un-protonated species of the Re(I) complex, which prevails in aqueous solutions at pH = 7, revealed that the band centered at λ_{max} = 252 nm consists mainly of intra ligand electronic transitions of 4,4′-bpy with some contributions of the Re(I) center. On the other hand, the band at 293 nm is a $\mathrm{MLLCT}_{\mathrm{Re(CO)_3 \rightarrow bpy\text{-}5,5'\text{-}diCOO}}$. The band at 317 is predicted as a sum of intra ligand transitions of bpy-5,5′-diCOO and 4,4′-bpy. However, the band at 332 nm, is mainly a $\mathrm{MLLCT}_{\mathrm{Re(CO)_3 \rightarrow 4,4'\text{-}bpy}}$. The lowest energy band, centered at λ_{max} ~360 nm, is predicted as a $\mathrm{MLLCT}_{\mathrm{Re(CO)_3 \rightarrow bpy\text{-}5,5'\text{-}diCOO}}$ electronic transition [22]. In this paper we have extended the TD-DFT calculations on the $[(4,4'\text{-bpy})\mathrm{Re(CO)_3(bpy\text{-}5,5'\text{-}diCOO)}]^-$ complex to the set of $CHCl_3$, CH_2Cl_2, CH_3CN, EtOH, MeOH solvents, with the purpose of understanding the role played by the solvent in the photophysical proper-

UNCORRECTED PROOF

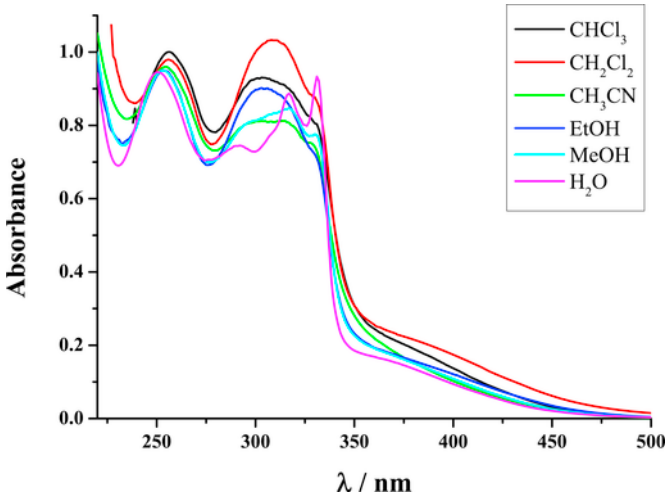

Fig. 1. Solvent effects on the UV-vis spectrum of $Bu_4N[(4,4'\text{-bpy})Re(CO)_3(bpy\text{-}5,5'\text{-diCOO})]$ complex.

ties of the $[(4,4'\text{-bpy})Re(CO)_3(bpy\text{-}5,5'\text{-diCOO})]^-$ complex. In the following section, TD-DFT results corresponding to the lowest energy band of the Re(I) complex will be discussed in detail, as the electronic transitions in this near UV-vis energy region are the ones responsible of the observed luminescence of the Re(I) complex (communicated in the Steady state and time resolved luminescence section, see below). The calculated TD-DFT results in the 300–400 nm region are summarized in Table 1 for the $[(4,4'\text{-bpy})Re(CO)_3(bpy\text{-}5,5'\text{-diCOO})]^-$ complex in $CHCl_3$, CH_2Cl_2, CH_3CN, EtOH, MeOH and H_2O. The main molecular orbitals (MOs) involved in the electronic transitions are H-7, H-6, H-5, H-3, H-2, L and L+1. Fig. 2 shows spatial plots of those MOs in H_2O, which provide interesting insights to the electronic transitions. Similar MO plots are observed in the organic solvents (not shown). In H_2O, there are four calculated electronic transitions. The lowest energy transition, calculated at λ_{calc} = 370.8 nm, corresponds to a $MLLCT_{Re(CO)_3 \rightarrow bpy\text{-}5,5'\text{-diCOO}}$ (a delocalized $Re(CO)_3 \rightarrow$bpy-5,5′-diCOO charge transfer transition). At λ_{calc} = 337.4 nm appears an electronic transition which is mainly a sum of different $LLCT_{bpy\text{-}5,5'\text{-diCOO} \rightarrow 4,4'\text{-bpy}}$ with minor contributions of $MLLCT_{Re(CO)_3 \rightarrow 4,4'\text{-bpy}}$. At λ_{calc} = 327.4 nm an $MLLCT_{Re(CO)_3 \rightarrow 4,4'\text{-bpy}}$ appears. The highest energy transition appears at 314.7 nm as an admixture of IL(bpy-5,5′-diCOO), IL(4,4′-bpy) and $MLLCT_{Re(CO)_3 \rightarrow 4,4'\text{-bpy}}$ excitations. In the organic solvents, the $LLCT_{bpy\text{-}5,5'\text{-diCOO} \rightarrow 4,4'\text{-bpy}}$ has disappeared and only the $MLLCT_{Re(CO)_3 \rightarrow bpy\text{-}5,5'\text{-diCOO}}$ and $MLLCT_{Re(CO)_3 \rightarrow 4,4'\text{-bpy}}$ electronic transitions are present. The calculated wavelength, λ_{calc}, for the $MLLCT_{Re(CO)_3 \rightarrow bpy\text{-}5,5'\text{-diCOO}}$ transition is rather insensitive to the polarity of the solvent. However, λ_{calc} for $MLLCT_{Re(CO)_3 \rightarrow 4,4'\text{-bpy}}$ experiences a bathochromic shift as the dielectric constant of the solvent, ε_r, decreases. Fig. 3a shows the dependence of the calculated dipole moment of the Re(I) complex, μ, on the solvent dielectric constant. It is observed that μ increases from around 13.5 D in solvents of low polarity like $CHCl_3$ to nearly 15.6 D in H_2O. This dependence of μ upon ε_r could imply that a polar solvent shifts the ground state of the Re(I) complex toward greater charge separation, while a nonpolar solvent shifts it toward a less polar structure. This effect has been previously reported [43]. Moreover, the vector of the dipole moment points along the axial axis (μ vector components in $CHCl_3$: X = −13.5029, Y = −0.3281 and Z = −1.2967) and is nearly perpendicular to the equatorial plane of the molecule. Fig. 3b shows that a

Table 1
Solvent effects on the calculated absorption data for $[(4,4'\text{-bpy})Re(CO)_3(bpy\text{-}5,5'\text{-diCOO})]^-$ in the 310–400 nm wavelength region.

Solvent	ε_r	λ_{calc}/nm (f_{osc})	Main electronic transitions (% coefficients)	Main character	%CT
H_2O	78.3553	314.7 (0.2059)	H-9 → L (49%), H-10 → L+1 (32%), H-8 → L+1 (10%)	IL(bpy-5,5′-diCOO), IL(4,4′-bpy), $MLLCT_{Re(CO)_3 \rightarrow 4,4'\text{-bpy}}$	–
		327.4 (0.1569)	H-6 → L+1 (73%), H-7 → L+1 (8%), H-5 → L+1 (4%), H-2 → L+1 (6%)	$MLLCT_{Re(CO)_3 \rightarrow 4,4'\text{-bpy}}$	46.1
		337.4 (0.0666)	H-6 → L+1 (11%), H-5 → L+1 (26%), H-3 → L+1 (25%), H-2 → L+1 (28%)	$LLCT_{dcbpy \rightarrow 4,4'\text{-bpy}}$	–
		370.8 (0.0782)	H-6 → L (80%), H-7 → L (10%),	$MLLCT_{Re(CO)_3 \rightarrow bpy\text{-}5,5'\text{-diCOO}}$	47.5
CH_3CN	35.688	312.2 (0.3674)	H-9 → L (83%)	IL(bpy-5,5′-diCOO)	–
		328.0 (0.1774)	H-6 → L+1 (85%)	$MLLCT_{Re(CO)_3 \rightarrow 4,4'\text{-bpy}}$	45.1
		369.3 (0.0825)	H-6 → L (91%)	$MLLCT_{Re(CO)_3 \rightarrow bpy\text{-}5,5'\text{-diCOO}}$	47.0
MeOH	32.613	314.8 (0.1954)	H-9 → L (46%), H-10 → L+1 (32%), H-8 → L+1 (13%)	IL(bpy-5,5′-diCOO), IL(4,4′-bpy), $MLLCT_{Re(CO)_3 \rightarrow 4,4'\text{-bpy}}$	–
		329.8 (0.1835)	H-6 → L+1 (81%)	$MLLCT_{Re(CO)_3 \rightarrow 4,4'\text{-bpy}}$	48.7
		371.1 (0.0817)	H-6 → L (84%), H-7 → L (10%)	$MLLCT_{Re(CO)_3 \rightarrow bpy\text{-}5,5'\text{-diCOO}}$	50.3
EtOH	24.852	312.5 (0.2962)	H-9 → L (67%), H-4 → L+2 (12%)	IL(bpy-5,5′-diCOO)	–
		329.6 (0.1911)	H-6 → L+1 (88%)	$MLLCT_{Re(CO)_3 \rightarrow 4,4'\text{-bpy}}$	47.1
		369.5 (0.0859)	H-6 → L (93%)	$MLLCT_{Re(CO)_3 \rightarrow bpy\text{-}5,5'\text{-diCOO}}$	48.6
CH_2Cl_2	8.93	316.0 (0.3579)	H-9 → L (83%)	IL(bpy-5,5′-diCOO)	–
		338.2 (0.2123)	H-6 → L+1 (61%), H-7 → L+1 (33%)	$MLLCT_{Re(CO)_3 \rightarrow 4,4'\text{-bpy}}$	54.9
		370.9 (0.0862)	H-6 → L (59%), H-7 → L (37%)	$MLLCT_{Re(CO)_3 \rightarrow bpy\text{-}5,5'\text{-diCOO}}$	53.6
$CHCl_3$	4.7113	316.2 (0.4087)	H-9 → L (77%)	IL(bpy-5,5′-diCOO)	–
		345.9 (0.2085)	H-7 → L+1 (87%)	$MLLCT_{Re(CO)_3 \rightarrow 4,4'\text{-bpy}}$	55.0
		369.1 (0.086)	H-7 → L (89%)	$MLLCT_{Re(CO)_3 \rightarrow bpy\text{-}5,5'\text{-diCOO}}$	53.4

correlation exists between the energy of the $MLLCT_{Re(CO)_3 \rightarrow 4,4'\text{-bpy}}$

UNCORRECTED PROOF

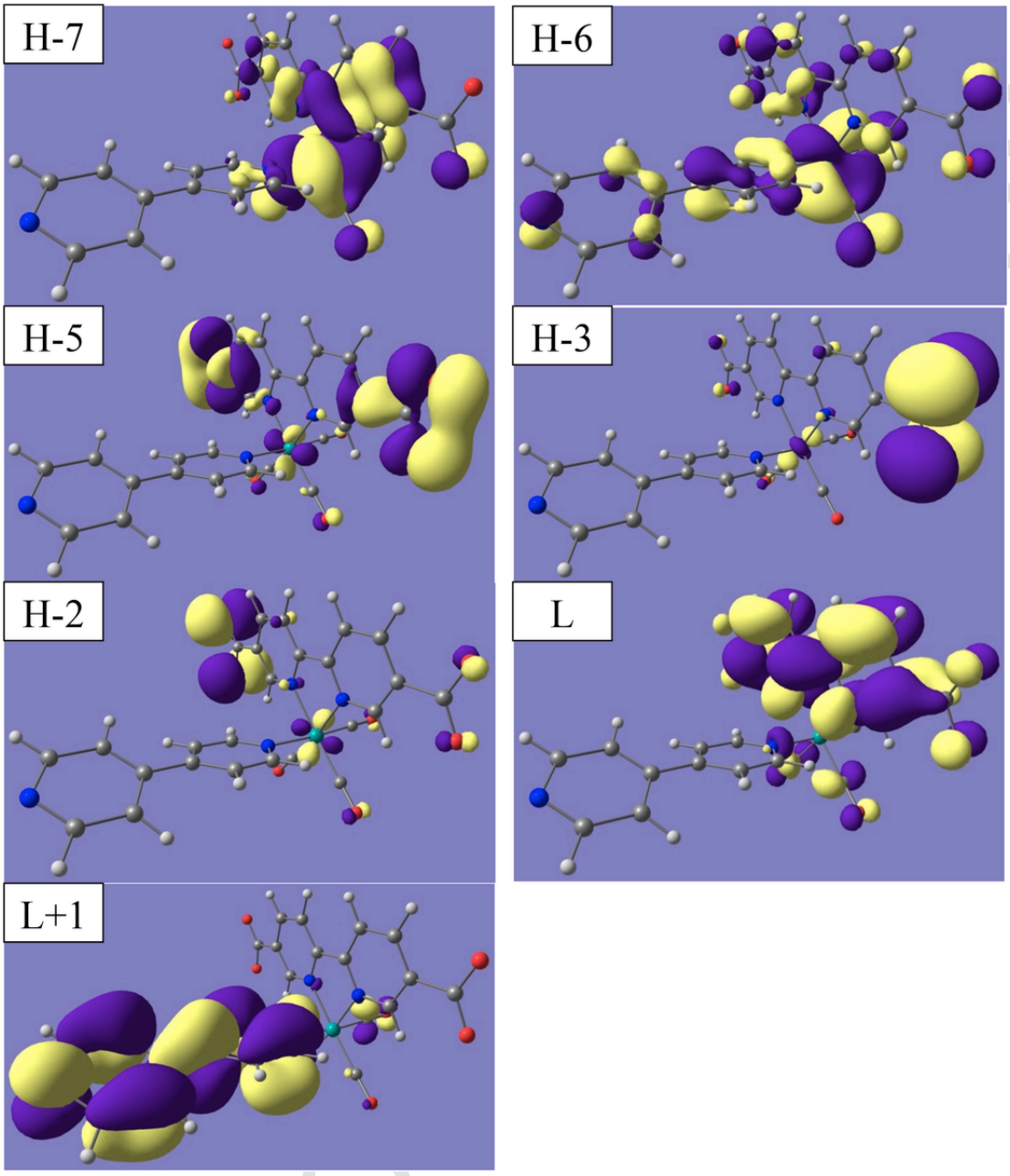

Fig. 2. Frontier MO plots of H-7, H-6, H-5, H-3, H-2, L and L+1 in H_2O (isovalue = 0.02) at the B3LYP/LanL2DZ level of theory. See text for details.

which the whole molecule can be split for analysis. The following fragments were defined: (i) Re atom, (ii) the three carbonyls, (iii) 4,4′-bipyridine (4,4′-bpy) and (iv) 2,2′-bipyridine-5,5′-dicarboxylate (bpy-5,5′-diCOO). Table 2 lists the orbital percentage composition of the relevant MOs of $[(4,4'\text{-bpy})Re(CO)_3(\text{bpy-}5,5'\text{-diCOO})]^-$ in the six solvents studied based on the fragments defined above. With the aid of those percentage compositions we calculated the percentages of charge transfer (CT(%)) of Table 1 using eq. (3)-5. The CT(%) for both $MLLCT_{Re(CO)_3 \rightarrow 4,4'\text{-bpy}}$ and $MLLCT_{Re(CO)_3 \rightarrow \text{bpy-}5,5'\text{-diCOO}}$ decreases as the solvent polarity increases, see Table 1 and Fig. S1. This is due to two facts. On the one hand, the percentage composition of Re orbitals in H-7 is higher than in H-6 in H_2O, CH_3CN, MeOH and EtOH while in CH_2Cl_2 and $CHCl_3$ both H-6 and H-7 have similar percentage contributions of Re orbitals. On the second hand, the main contributions to $MLLCT_{Re(CO)_3 \rightarrow 4,4'\text{-bpy}}$ and $MLLCT_{Re(CO)_3 \rightarrow \text{bpy-}5,5'\text{-diCOO}}$ transitions come from H-6 in H_2O, CH_3CN, MeOH and EtOH while in CH_2Cl_2 both H-6 and H-7 MOs participate and in $CHCl_3$ H-7 is the main MO involved in both electronic transitions. Fig. S2 shows the simulated absorption spectra for all the solvents under study. No significant differences in the calculated absorption spectra were encountered when the level of theory was switched between B3LYP/LanL2DZ, M06/LanL2DZ and PBE0/6-311++G(d,p)/LanL2TZ(f). The comparison with the experimental spectra of Fig. 1 is quite satisfactory and the simulated spectra follow the observed absorptions with reasonable accuracy both in position and relative intensities. Moreover, the bathochromic shift experienced by the wavelength corresponding to the lowest energy band of Fig. 1 is reproduced by the spectra of Fig. S2. Interestingly, the solvent effect on

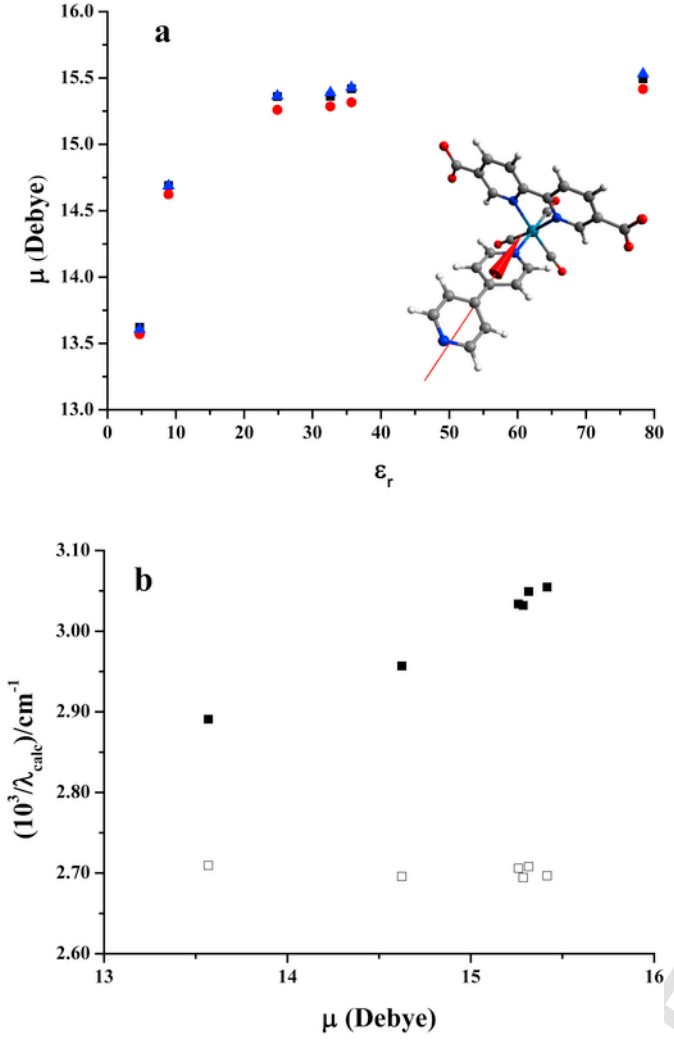

Fig. 3. a: dependence of the calculated dipole moment of $[(4,4'\text{-bpy})Re(CO)_3(bpy\text{-}5,5'\text{-diCOO})]^-$, μ, on the solvent dielectric constant, ε_r. μ was calculated at the (■) M06/LanL2DZ (●), B3LYP/LanL2DZ and (▲) PBE0/6-311++G(d,p)/LanL2TZ(f) level of theory. The red arrow displays the direction of μ which is nearly parallel to the axial 4,4′-bpy ligand of $[(4,4'\text{-bpy})Re(CO)_3(bpy\text{-}5,5'\text{-diCOO})]^-$ complex. **3b**: Calculated energy of the (■) $MLLCT_{Re(CO)_3 \rightarrow 4,4'\text{-bpy}}$ and (□) $MLLCT_{Re(CO)_3 \rightarrow bpy\text{-}5,5'\text{-diCOO}}$ transitions vs μ at the B3LYP/LanL2DZ level of theory. (For interpretation of the references to colour in this figure legend, the reader is referred to the web version of this article.)

the highest energy band of Fig. 1 (a bathochromic shift on λ_{max} as the polarity of the solvent is decreased from 252 nm in H_2O to 256 nm in $CHCl_3$) is also observed in Fig. S2. However, the calculated λ_{max} for the highest energy band in CH_3CN and EtOH deviates from that trend and appear at the shortest wavelengths. This disparity was observed either with B3LYP, M06 or PBE0 functional.

3.2. Steady state and time resolved luminescence

The steady state luminescence of $Bu_4N[(4,4'\text{-bpy})Re(CO)_3(bpy\text{-}5,5'\text{-diCOO})]$ shows a strong solvent dependence. Fig. 4 shows the emission spectrum of N_2-deaerated solutions of the Re(I) complex in the six solvents with $\lambda_{exc} = 360$ nm. When the spectrum was taken in water the emission occurred peaking at $\lambda_{max} = 435$ nm. In the aprotic solvents the maximum of the luminescence spectrum occurred at 604, 595 and 570 nm for CH_3CN, CH_2Cl_2 and $CHCl_3$, respectively. However, in MeOH and EtOH, two peaks were observed; one at 425 and the other around 600 nm. On the other hand, $Bu_4N[(4,4'\text{-bpy})Re(CO)_3(bpy\text{-}5,5'\text{-diCOO})]$ is a weak luminophore with Φ_{em} ranging between 10^{-3} and 10^{-2}.

A sum of two exponentials were required to achieve a satisfactory fit of the emission decay profiles of the Re(I) complex solutions in H_2O, MeOH, EtOH and CH_3CN, while 3 components were required for the satisfactory analysis of the traces in CH_2Cl_2 and $CHCl_3$. A fast component decay, $\tau_1 \sim 1$–6 ns, shows no correlation on the solvent polarity. However, the second component decay lifetime, $\tau_2 \sim 10$–25 ns, increases with the polarity of the solvent. The longest third component decay, $\tau_3 \sim 150$–250 ns, was only observed in CH_2Cl_2 and $CHCl_3$. The presence of O_2 in the solutions quenched both the steady state and time resolved luminescence of the Re(I) complex in all the solvents. For instance, in CH_3CN, $\tau_2 = 13.2$ ns in N_2 equilibrated solutions while $\tau_2 = 7.5$ ns in air equilibrated solutions. A similar decrease of τ with the increase of O_2 concentration was observed in the other solvents, see Table 3.

Table 2
Composition (% character) of relevant Molecular Orbitals of $[(4,4'\text{-bpy})Re(CO)_3(bpy\text{-}5,5'\text{-diCOO})]^-$ calculated with the AOMIX program.

Solvent	MO	Re	3COs	4,4′-bpy	Bpy-5,5′-diCOO
H_2O	H−7	58.92	26.23	1.33	13.52
	H−6	54.38	24.03	9.38	12.21
	L	2.07	4.16	0.59	93.18
	L+1	0.87	2.64	95.85	0.65
CH_3CN	H−7	58.83	26.57	0.86	13.74
	H−6	53.80	24.15	9.89	12.16
	L	2.06	4.22	0.64	93.08
	L+1	0.92	2.87	95.45	0.75
MeOH	H−7	59.11	26.31	1.28	13.31
	H−6	55.22	24.41	9.27	11.10
	L	2.09	4.18	0.60	93.13
	L+1	0.87	2.61	95.89	0.64
EtOH	H−7	58.90	26.59	0.89	13.62
	H−6	54.36	24.37	9.74	11.53
	L	2.07	4.23	0.67	93.03
	L+1	0.92	2.86	95.47	0.75
CH_2CL_2	H−7	58.61	25.91	3.26	12.22
	H−6	57.58	25.39	6.37	10.66
	L	2.16	4.28	0.66	92.89
	L+1	0.86	2.52	96.04	0.57
$CHCl_3$	H−7	57.91	25.30	7.53	9.26
	H−6	58.60	25.94	1.28	14.18
	L	2.25	4.39	0.77	92.59
	L+1	0.86	2.45	96.14	0.54

UNCORRECTED PROOF

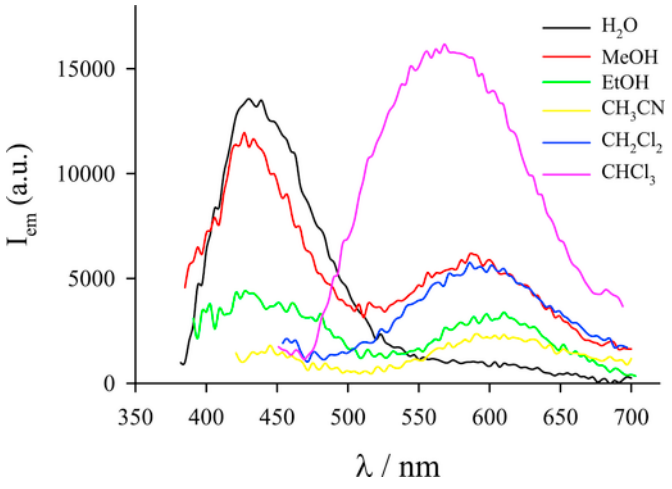

Fig. 4. Solvent dependence of $Bu_4N[(4,4'\text{-bpy})Re(CO)_3(bpy\text{-}5,5'\text{-diCOO})]$ emission spectrum: H_2O, MeOH, EtOH, CH_3CN, CH_2Cl_2 and $CHCl_3$. Solutions were deaerated by bubbling N_2. Excitation wavelength is 360 nm.

Table 3
Re(I) complex luminescence lifetimes (λ_{exc} = 341 nm, % relative amplitudes between parenthesis) and luminescence quantum yields in different solvents. % Relative amplitudes are calculated as $100.B_i\tau_i/(\sum_i B_i\tau_i)$, where B_i represents the pre-exponential factor corresponding to τ_i decay component of the luminescence.

Solvent	λ_{max}/nm	τ (N_2)/ns	τ (air)/ns	Φ_{em}(N_2) (±10%)
H_2O	435	τ_1:1.7 (6%), τ_2:21.4 (94%)	τ_1:1.3 (6%), τ_2:20.8 (94%)	3.4×10^{-3}
MeOH	425	τ_1:5.9 (62%), τ_2:22.9 (48%)	τ_1:4.2 (54%), τ_2:11.4 (46%)	4.3×10^{-3}
	590	τ_1:4.7 (70%), τ_2:20.0 (30%)	τ_1:3.4 (57%), τ_2:13.8 (43%)	
EtOH	425	τ_1:5.5 (65%), τ_2:14.6 (35%)	τ_1:2.8 (38%), τ_2:9.3 (62%)	2.0×10^{-3}
	604	τ_1:4.8 (65%), τ_2:23.1 (35%)	τ_1:4.1 (80%), τ_2:20.0 (20%)	
CH_3CN	435	τ_1:3.7 (30%), τ_2:13.2 (70%)	τ_1:1.5 (33%), τ_2:7.5 (67%)	1.2×10^{-3}
	604	τ_1:3.6 (61%), τ_2:12.2 (39%)	τ_1:3.1 (52%), τ_2:10.3 (48%)	
CH_2Cl_2	595	τ_1:2.4 (10%) τ_2:10.0 (52%) τ_3:160 (38%)	τ_1:1.8 (12%) τ_2: 9.6 (66%) τ_3:116 (22%)	2.9×10^{-3}
$CHCl_3$	570	τ_1:3.0 (13%) τ_2:13.5 (41%) τ_3:239 (46%)	τ_1:2.3 (8%) τ_2:13.2 (48%) τ_3:191 (44%)	1.1×10^{-2}

The luminescence lifetime of the related complex $Re(CO)_3(4,4'\text{-bpy})_3^+$ corresponding to the radiative and non-radiative decay of the $MLLCT_{Re(CO)_3 \rightarrow 4,4'\text{-bpy}}$ is 93 ns in CH_2Cl_2 and 439 ns in CH_3CN [44]. On the other hand, for the $[Re(4,4'\text{-bpy})(CO)_3(bpy\text{-}4,4'\text{-diCOOH})]^+$ complex in aqueous solutions, a pH dependent lifetime ranging from $\tau \sim 50$ ns (at pH~1) to $\tau \sim 90$ ns (at pH~10) was reported [45], though no assignment to whether it corresponded to an $MLLCT_{Re(CO)_3 \rightarrow bpy\text{-}4,4'\text{-diCOO}}$ or a $MLLCT_{Re(CO)_3 \rightarrow 4,4'\text{-bpy}}$ excited state was made on that report. On this basis, solvent effects on the steady state and time resolved luminescence of the $Bu_4N[(4,4'\text{-bpy})Re(CO)_3(bpy\text{-}5,5'\text{-diCOO})]$ complex can be accounted by the coexistence of $^3MLLCT_{Re(CO)_3 \rightarrow 4,4'\text{-bpy}}$, $^3MLLCT_{Re(CO)_3 \rightarrow bpy\text{-}5,5'\text{-diCOO}}$ and ^{1}IL excited states. While the shortest lifetime (2–5 ns in Table 3) should be attributed to the ^{1}IL (4,4′-bpy and/or bpy-5,5′-diCOO based) excited states, it is uncertain to make a clear assignment of the ~20 ns and ~200 ns lifetimes of Table 3 to each of the $^3MLLCT_{Re(CO)_3 \rightarrow 4,4'\text{-bpy}}$ or $^3MLLCT_{Re(CO)_3 \rightarrow bpy\text{-}5,5'\text{-diCOO}}$ excited states. However, the triplet character of the emitting excited state is manifested in the intrinsic quenching effect by O_2 in organic solvents.

3.3. Singlet oxygen generation and LIOAS experiments

Singlet oxygen generation in D_2O or CH_3CN solutions could not be detected under our experimental conditions. The fact that $^1O_2$ ($^1\Delta_g$) is not generated with this complex is related to the low ^{3}MLLCT emission in those solvents. This is in agreement with our previous results in relation to the photosensitized generation of singlet oxygen from structurally related Re(I) complexes: $^1O_2$ ($^1\Delta_g$) generation was not observed when the luminescence quantum yields of the Re(I) complexes were as low as $\Phi_{em} \sim 10^{-3}$ [23,24].

The photoacoustic signal in both solvents showed the same behavior: no time shift or changes of shape, with respect to the calorimetric reference signal (See Inset of Fig. 5 for aqueous solutions). Linear relationships in both solvents were obtained between the amplitude of the first optoacoustic signal (H) and the excitation fluence (F) for samples and references at various A, in a fluence range between 1 and 30 J/m^2. The ratio between the slopes of these lines for sample and reference yielded the values of α for the samples. For the complex in CH_3CN solution, see Fig. 5, the slopes were independent on the specific atmosphere and were the same that the CR measured at the same experimental conditions, as shown in Fig. 5. From these plots, considering that $\alpha_R = 1$ for CR, the α values were calculated for the complex in both solvents. Therefore, $\alpha = 1.00 \pm 0.04$ were obtained in aqueous and in CH_3CN solutions (either under N_2 or O_2 atmosphere). Consequently, this complex released to the medium all the absorbed energy as prompt heat (integrated by the transducer) in processes faster than $\tau_R/5$. These values combined with fluorescence data and singlet oxygen quantum yield production fit the energy balance of eq. (6) [24,25]:

$$E_a = \Phi_{em} E_{em} + \alpha E_a + \Phi_{st} E_{st} \quad (6)$$

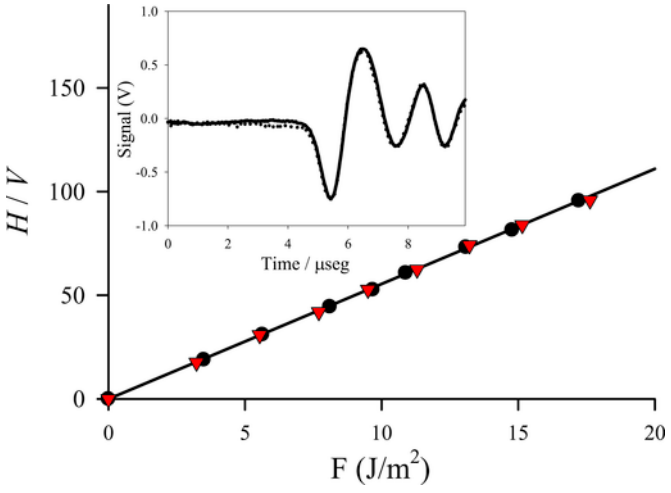

Fig. 5. Amplitude of the photoacoustic signals as a function of laser fluence for aqueous solutions: New Coccine (CR, ●), Re(I) complex (▼). Inset: Normalized photoacoustic signals of aqueous solutions for the CR (dotted line) and the Re(I) complex (solid line) with matched absorbances (0.167 ± 0.002).

UNCORRECTED PROOF

where E_{em} is the "0–0" luminescence energy, E_a is the molar energy of the laser pulse (hc/λ_{exc}), E_{st} is the molar energy content of the species formed with a quantum yield Φ_{st} which stores energy for a time longer than the heat integration time and decays with a lifetime τ. When singlet oxygen acts as storing species, the corresponding values for this species are $\Phi_{st} = \Phi_{\Delta}$ and $\tau = \tau_{\Delta}$.

3.4. Triplet energy calculations

Triplet emission energies were computed by optimizing the geometry at their excited state with analytic TD-DFT calculations utilizing B3LYP functional and LanL2DZ basis set. This approach provided the vertical transition energy of the lowest triplet excited state at its optimal geometry. In addition, we also used a Δ(SCF) method. While TD-DFT directly computes the vertical transition energy of the lowest triplet state at its optimal geometry, the Δ(SCF) method is based on the difference in total energies between self-consistent calculations of the ground singlet and triplet electronic configurations and approximates "0–0" transitions. The validation of both techniques relies on the consistency between Δ(SCF) and TD-DFT results [46,47]. All calculations were carried out in the presence of $CHCl_3$ as a solvent through the PCM to better simulate experimental results. In unrestricted TD-DFT calculations, the choice of the triplet of interest (T_n) was based on the nature of the lowest energy singlet-singlet transition (H−7 → L see Table 1) in $CHCl_3$. Then, the optimized geometry of T_n and the calculated wavelength, λ_{calc} = 491.4 nm, corresponding to a H−6 → (H_α, $L+1_\beta$) vertical transition were obtained. Fig. 6 shows frontier MO plots of the triplet's H_α and $L+1_\beta$ along with the singlet's H−6. H_α is a MO centered on the bpy-5,5′-diCOO ligand while $L+1_\beta$ is centered on the 4,4′-bpy ligand. Therefore, the S_0-T_n transition should be viewed as a delocalized MLLCT transition where the electronic charge is transferred from $Re(CO)_3$ moiety to both 4,4′-bpy and bpy-5,5′-diCOO ligands. The S_0-T_n energy difference computed as Δ(SCF) energy where T_n and the S_0 structures are at the S_0 (ΔE_1 (T_n@T_n:S_0@S_0)) and T_n (ΔE_2 (T_n@T_n:S_0@T_n)) relaxed geometry are reported in Table 4, at the B3LYP/LanL2DZ/PCM($CHCl_3$), PBE0/LanL2DZ/PCM($CHCl_3$) and M06/LanL2DZ/PCM($CHCl_3$) level of theory. ΔE_1 values are too "blue" compared to the experimental ones (*vide supra*) while ΔE_2 are higher by 0.2–0.3 eV. Table 5 shows selected bond lengths and angles around Re atom for the ground (S_0) and triplet (T_n) state computed at the B3LYP/LanL2DZ/PCM($CHCl_3$) level of theory (See Scheme 1 for the numbering of atoms in Table 5). It is observed that in the triplet state the Re-N1, Re-N2 and Re-N24 distances are shortened while Re-C46, Re-C47 and Re-C48 distances are elongated relative to the ground state. This is in agreement with the nature of the ^{3}MLLCT where formally the charge on the Re center is 2 + and a negative charge is located over the azine ligand, increasing thus the electrostatic attraction between the Re center and the coordinated ligand, with a concomitant decrease in Re—N bonds distances. The increase of Re—C bonds distances points to a steric effect imposed by the approaching of the azine ligands. It is interesting to note that the Re-N1 and Re-N2 distances are shortened by 0.062 Å while the Re-N24 distance is only shortened by 0.023 Å. The elongation of Re-C46, Re-C47 and Re-C48 distances is 0.040, 0.039 and 0.037 Å, respectively, i.e. very similar for the three Re—C bonds.

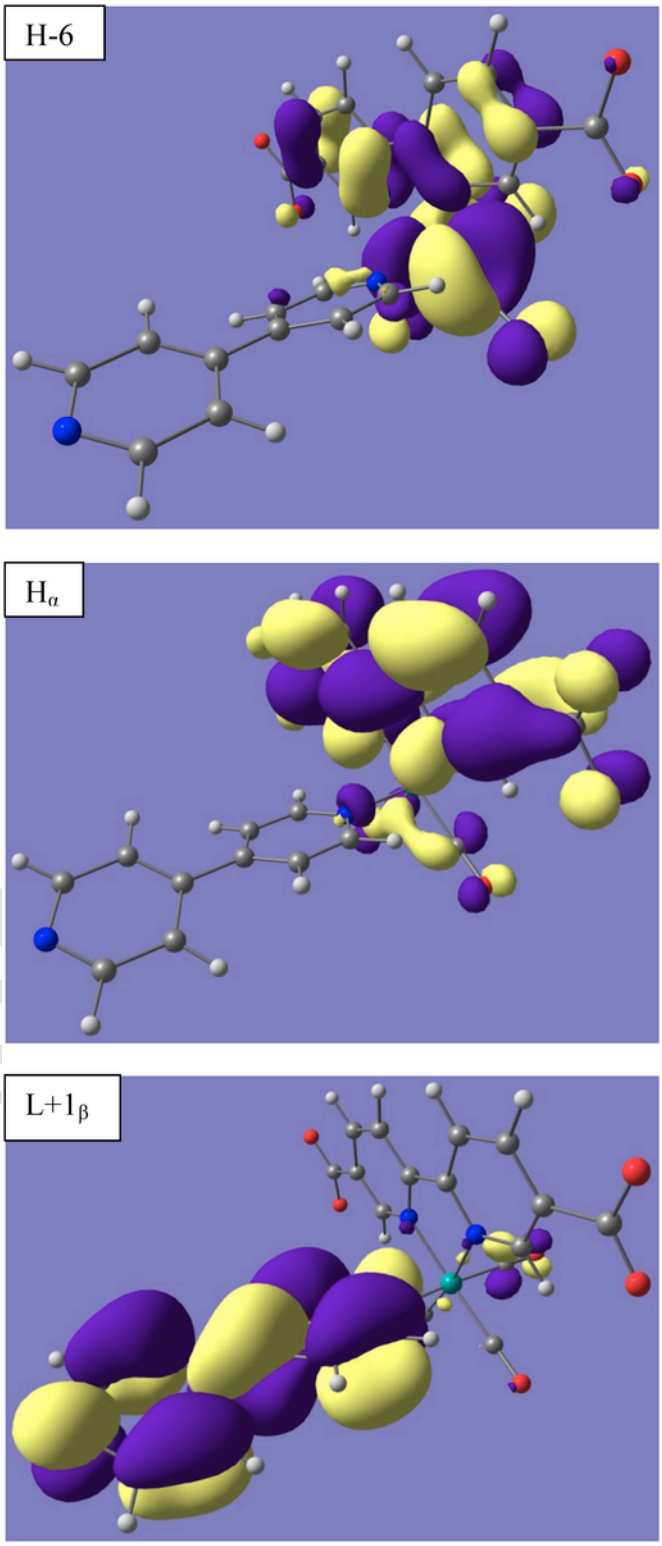

Fig. 6. Frontier MO plots of the triplet's H_α and $L+1_\beta$ along with the singlet's H-6 (isovalue = 0.02) of $[(4,4'\text{-bpy})Re(CO)_3(\text{bpy-}5,5'\text{-diCOO})]^-$ complex. See text for details.

UNCORRECTED

Table 4
Calculated wavelengths, λ_1 and λ_2, corresponding to the energy differences ΔE_1 and ΔE_2, respectively. $\Delta E(S_0 \rightarrow T_n)$ are computed as Δ(SCF) energy where T_n and the S_0 structures are at the S_0 ($\Delta E_1(T_n@T_n{:}S_0@S_0)$) and T_n ($\Delta E_2(T_n@T_n{:}S_0@T_n)$) relaxed geometry. All calculations were performed at the at B3LYP/LanL2DZ, PBE0/LanL2DZ or M06/LanL2DZ level of theory including solvents effects ($CHCl_3$) through the PCM.

	λ_1/nm	λ_2/nm
B3LYP	467.2	524.4
PBE0	442.2	497.1
M06	439.8	492.7

Table 5
Optimized geometrical parameters of S_0 and T_n for [(4,4′-bpy)Re(CO)$_3$(bpy-5,5′-diCOO)]$^-$. Bond lengths (Å) and angles (°) around the Re ion were calculated at the uB3-LYP/LanL2DZ/PCM ($CHCl_3$) level of theory.

	S_0	T_n
Bond lengths (Å)		
Re-N1	2.178	2.116
Re-N2	2.178	2.116
Re-N24	2.229	2.206
Re-C46	1.926	1.966
Re-C47	1.926	1.965
Re-C48	1.925	1.962
Bond angles (°)		
N1-Re-N2	75.7	78.0
N1-Re-N24	84.6	86.6
N1-Re-C46	172.6	171.8
N1-Re-C47	97.6	94.2
N1-Re-C48	92.6	96.5
N2-Re-N24	85.0	86.6
N2-Re-C46	97.5	94.2
N2-Re-C47	172.9	171.8
N2-Re-C48	92.3	96.4
C46-Re-N24	92.0	90.4
C46-Re-C47	89.0	93.4
C46-Re-C48	90.5	86.9
C47-Re-N24	92.0	90.5
C47-Re-C48	90.4	86.9
C48-Re-N24	176.5	176.1

4. Conclusions

The absorption spectrum as well as the steady state and time resolved luminescence of the Bu_4N[(4,4′-bpy)Re(CO)$_3$(bpy-5,5′-diCOO)] complex displays a marked solvent effect. The high energy absorption bands experience a bathochromic shift as the polarity of the solvent decreases. In addition to the bathochromic shift, the lowest energy band broadens. TD-DFT calculations allowed us to identify the main electronic transitions in the low energy region as $^1MLLCT_{Re(CO)_3 \rightarrow 4,4'\text{-bpy}}$ and $^1MLLCT_{Re(CO)_3 \rightarrow \text{bpy-5,5'-diCOO}}$. The magnitude of the calculated dipole moment increases with the polarity of the solvent. Besides, the energy of $^1MLLCT_{Re(CO)_3 \rightarrow 4,4'\text{-bpy}}$ increases also with solvent polarity increase. However, the energy of the $^1MLLCT_{Re(CO)_3 \rightarrow \text{bpy-5,5'-diCOO}}$ transition is rather insensitive to the solvent polarity. This disparity is attributed to the fact that the $^1MLLCT_{Re(CO)_3 \rightarrow 4,4'\text{-bpy}}$ transition is nearly parallel to the orientation of the dipole moment while the $^1MLLCT_{Re(CO)_3 \rightarrow \text{bpy-5,5'-diCOO}}$ transition is almost perpendicular to it. Both electronic transitions show a decrease of their CT(%) with increasing solvent polarity. The solvent effect on the position of the luminescence maximum and lifetime is consistent with the radiative and non-radiative deactivation of ^1IL, $^3MLLCT_{Re(CO)_3 \rightarrow 4,4'\text{-bpy}}$ and $^3MLLCT_{Re(CO)_3 \rightarrow \text{bpy-5,5'-diCOO}}$ excited states. No singlet oxygen generation was detected either in D_2O or CH_3CN. LIOAS experiments showed that after photonic excitation all the absorbed energy was released to the medium as prompt heat in agreement with the low quantum yield of luminescence and the absence of any long-lived energy storage species. Unrestricted TD-DFT calculations were successfully applied to the triplet species. It is observed that in the triplet state the Re—N distances are shortened while Re—C distances are elongated relative to the ground state, in agreement with the CT nature of the triplet state. The calculated Δ(SCF) energies were somewhat "blue" shifted relative to the experimental ones.

Acknowledgments

This work was supported in part by ANPCyT (PICT 1435), CONICET (PIP 0389), and Universidad Nacional de La Plata (UNLP X611) of Argentina. H.H.M.S. and F.R. thank CONICET for research scholarships. G.T.R. and E.W. are Research Members of CONICET (Argentina). P.D.G is a Research Member of CICBA (Argentina).

Appendix A. Supplementary data

Supplementary data related to this article can be found at http://dx.doi.org/10.1016/j.jorganchem.2016.05.012.

References

[1] M.A. Fox, M. Chanon, Photoinduced Electron Transfer, Elsevier, Amsterdam, 1988.
[2] V. Balzani, F. Bolletta, M. Gandolfi, M. Maestri, Bimolecular electron transfer reactions of the excited states of transition metal complexes, In: Organic Chemistry and Theory, Springer, Berlin/Heidelberg, 1978, pp. 1–64.
[3] M. Grätzel, Energy Resources Through Photochemistry and Catalysis, Academic Press, New York, 1983.
[4] K. Kalyanasundaram, Photophysics, photochemistry and solar energy conversion with tris(bipyridyl)ruthenium(II) and its analogues, Coord. Chem. Rev. 46 (1982) 159–244.
[5] K. Kalyanasundaram, M. Grätzel, Photosensitization and Photocatalysis Using Inorganic and Organometallic Compounds, Kluwer Academic Publishers, Dordrecht, 1993.
[6] L. Sacksteder, M. Lee, J.N. Demas, B.A. DeGraff, Long-lived, highly luminescent rhenium(I) complexes as molecular probes: intra- and intermolecular excited-state interactions, J. Am. Chem. Soc. 115 (1993) 8230–8238.
[7] V.W.-W. Yam, K.M.-C. Wong, V.W.-M. Lee, K.K.-W. Lo, K.-K. Cheung, Synthesis, photophysics, ion-binding studies, and structural characterization of organometallic rhenium(I) crown complexes, Organometallics 14 (1995) 4034–4036.
[8] D.I. Yoon, C.A. Berg-Brennan, H. Lu, J.T. Hupp, Synthesis and preliminary photophysical studies of intramolecular electron transfer in crown-linked donor-(chromophore-) acceptor complexes, Inorg. Chem. 31 (1992) 3192–3194.
[9] M.-W. Louie, T.T.-H. Fong, K.K.-W. Lo, Luminescent Rhenium(I) polypyridine fluorous complexes as novel trifunctional biological probes, Inorg. Chem. 50 (2011) 9465–9471.
[10] K. Lo, Exploitation of luminescent organometallic Rhenium(I) and iridium(III) complexes in biological studies, in: A.J. Lees (Ed.), Photophysics of Organometallics, Springer, Berlin/Heidelberg, 2010, pp. 73–114.
[11] K.K.-W. Lo, A.W.-T. Choi, W.H.-T. Law, Applications of luminescent inorganic and organometallic transition metal complexes as biomolecular and cellular probes, Dalton Trans. 41 (2012) 6021–6047.
[12] G.T. Ruiz, M.P. Juliarena, R.O. Lezna, E. Wolcan, M.R. Feliz, G. Ferraudi, Intercalation of fac-[(4,4′-bpy)ReI(CO) 3(dppz)]+, dppz = dipyridyl[3,2-a:2′3′-c] phenazine, in polynucleotides. on the UV-vis photophysics of the Re(i) intercalator and the redox reactions with pulse radiolysis-generated radicals, Dalton Trans. (2007) 2020–2029.
[13] S.P. Foxon, M.A.H. Alamiry, M.G. Walker, A.J.H.M. Meijer, I.V. Sazanovich, J.A. Weinstein, J.A. Thomas, Photophysical properties and singlet oxygen production by ruthenium(II) complexes of benzo[i]dipyrido[3,2-a:2′,3′-c]phenazine: spectroscopic and TD-DFT study, J. Phys. Chem. A 113 (2009) 12754–12762.
[14] J. Bhuvaneswari, A.K. Fathima, S. Rajagopal, Rhenium(I)-based fluorescence resonance energy transfer probe for conformational changes of bovine serum albumin, J. Photochem. Photobiol. A 227 (2012) 38–44.
[15] M. Cattaneo, F. Fagalde, C.D. Borsarelli, N.S.E. Katz, Improvement of the dynamic range of pH sensing by using a luminescent tricarbonylpolypyridylrhe-

UNCORRECTED PROOF

nium(i) complex with three different protonation sites, Inorg. Chem. 48 (2009) 3012–3017.
[16] M. Cattaneo, F. Fagalde, N.E. Katz, Proton-induced luminescence of mono- and dinuclear rhenium(I) tricarbonyl complexes containing 4-pyridinealdazine, Inorg. Chem. 45 (2006) 6884–6891.
[17] M. Cattaneo, F. Fagalde, N.E. Katz, C.D. Borsarelli, T. Parella, pH-Induced luminescence changes of chromophore-quencher tricarbonylpolypyridylrhenium(I) complexes with 4-pyridinealdazine, (Eur. J. Inorg. Chem. 34/2007), Eur. J. Inorg. Chem. 2007 (2007). 5309–5309.
[18] B. Higgins, B.A. DeGraff, J.N. Demas, Luminescent transition metal complexes as sensors: structural effects on pH response, Inorg. Chem. 44 (2005) 6662–6669.
[19] R.-J. Lin, K.-S. Lin, I.J. Chang, Photophysical properties of tricarbonyl(histidine)(diimine)rhenium(I) complexes in aqueous solution, Inorg. Chim. Acta 242 (1996) 179–183.
[20] S.C. Bottorff, A.L. Moore, A.R. Wemple, D.-K. Bučar, L.R. MacGillivray, P.D. Benny, pH-Controlled coordination mode rearrangements of "clickable" huisgen-based multidentate ligands with [MI(CO)3]+ (M = Re, 99mTc), Inorg. Chem. 52 (2013) 2939–2950.
[21] F. Ragone, G.T. Ruiz, O.E. Piro, G.A. Echeverría, F.M. Cabrerizo, G. Petroselli, R. Erra-Balsells, K. Hiraoka, F.S. García Einschlag, E. Wolcan, Water-soluble (pterin)rhenium(I) complex: synthesis, structural characterization, and two reversible protonation–deprotonation behavior in aqueous solutions, Eur. J. Inorg. Chem. 2012 (2012) 4801–4810.
[22] H.H. Martinez Saavedra, C.A. Franca, G. Petroselli, R. Erra-Balsells, G.T. Ruiz, E. Wolcan, A new zwitterionic, water soluble, Re(I) complex: synthesis, spectroscopic and computational characterization, J. Organomet. Chem. 745–746 (2013) 470–478.
[23] H.H. Martinez Saavedra, F. Ragone, G.T. Ruiz, P.M.D. Gara, E. Wolcan, Solvent dependent switching of 3MLLCT and 1IL luminescent states in [ClRe(CO)3(Bathocuproinedisulfonate)]2–: spectroscopic and computational study, J. Phys. Chem. A 118 (2014) 9661–9674.
[24] F. Ragone, H.H.M. Saavedra, P.M.D. Gara, G.T. Ruiz, E. Wolcan, Photosensitized generation of singlet oxygen from Re(I) complexes: a photophysical study using LIOAS and luminescence techniques, J. Phys. Chem. A 117 (2013) 4428–4435.
[25] S.E. Braslavsky, G.E. Heibel, Time-resolved photothermal and photoacoustic methods applied to photoinduced processes in solution, Chem. Rev. 92 (1992) 1381–1410.
[26] P. Van Haver, L. Viaene, M. Van der Auweraer, F.C. De Schryver, References for laser-induced opto-acoustic spectroscopy using UV excitation, J. Photochem. Photobiol. A 63 (1992) 265–277.
[27] S. Abbruzzetti, C. Viappiani, D.H. Murgida, R. Erra-Balsells, G.M. Bilmes, Non-toxic, water-soluble photocalorimetric reference compounds for UV and visible excitation, Chem. Phys. Lett. 304 (1999) 167–172.
[28] R. Schmidt, C. Tanielian, R. Dunsbach, C. Wolff, Phenalenone, a universal reference compound for the determination of quantum yields of singlet oxygen O2(1Δg) sensitization, J. Photochem. Photobiol. A 79 (1994) 11–17.
[29] P. Hohenberg, W. Kohn, Inhomogeneous electron gas, Phys. Rev. 136 (1964) B864–B871.
[30] W. Kohn, L.J. Sham, Self-consistent equations including exchange and correlation effects, Phys. Rev. 140 (1965) A1133–A1138.
[31] R.G. Parr, W. Yang, Density Functional Theory of Atoms and Molecules, Oxford University Press, 1989.
[32] R. Bauernschmitt, R. Ahlrichs, Treatment of electronic excitations within the adiabatic approximation of time dependent density functional theory, Chem. Phys. Lett. 256 (1996) 454–464.
[33] M.E. Casida, C. Jamorski, K.C. Casida, D.R. Salahub, Molecular excitation energies to high-lying bound states from time-dependent density-functional response theory: characterization and correction of the time-dependent local density approximation ionization threshold, J. Chem. Phys. 108 (1998) 4439–4449.
[34] R.E. Stratmann, G.E. Scuseria, M.J. Frisch, An efficient implementation of time-dependent density-functional theory for the calculation of excitation energies of large molecules, J. Chem. Phys. 109 (1998) 8218–8224.
[35] M.J. Frisch, G.W. Trucks, H.B. Schlegel, G.E. Scuseria, M.A. Robb, J.R. Cheeseman, G. Scalmani, V. Barone, B. Mennucci, G.A. Petersson, H. Nakatsuji, M. Caricato, X. Li, H.P. Hratchian, A.F. Izmaylov, J. Bloino, G. Zheng, J.L. Sonnenberg, M. Hada, M. Ehara, K. Toyota, R. Fukuda, J. Hasegawa, M. Ishida, T. Nakajima, Y. Honda, O. Kitao, H. Nakai, T. Vreven, J.J.A. Montgomery, J.E. Peralta, F. Ogliaro, M. Bearpark, J.J. Heyd, E. Brothers, K.N. Kudin, V.N. Staroverov, T. Keith, R. Kobayashi, J. Normand, K. Raghavachari, A. Rendell, J.C. Burant, S.S. Iyengar, J. Tomasi, M. Cossi, N. Rega, J.M. Millam, M. Klene, J.E. Knox, J.B. Cross, V. Bakken, C. Adamo, J. Jaramillo, R. Gomperts, R.E. Stratmann, O. Yazyev, A.J. Austin, R. Cammi, C. Pomelli, J.W. Ochterski, R.L. Martin, K. Morokuma, V.G. Zakrzewski, G.A. Voth, P. Salvador, J.J. Dannenberg, S. Dapprich, A.D. Daniels, O. Farkas, J.B. Foresman, J.V. Ortiz, J. Cioslowski, D.J. Fox, Gaussian 09, Revision A1, Gaussian, Inc., Wallingford CT, 2009.
[36] V. Barone, M. Cossi, Quantum calculation of molecular energies and energy gradients in solution by a conductor solvent model, J. Phys. Chem. A 102 (1998) 1995–2001.
[37] M. Cossi, V. Barone, Time-dependent density functional theory for molecules in liquid solutions, J. Chem. Phys. 115 (2001) 4708–4717.
[38] B. Mennucci, J. Tomasi, Continuum solvation models: a new approach to the problem of solute's charge distribution and cavity boundaries, J. Chem. Phys. 106 (1997) 5151–5158.
[39] D. Feller, The role of databases in support of computational chemistry calculations, J. Comput. Chem. 17 (1996) 1571–1586.
[40] K.L. Schuchardt, B.T. Didier, T. Elsethagen, L. Sun, V. Gurumoorthi, J. Chase, J. Li, T.L. Windus, Basis set exchange: a community database for computational sciences, J. Chem. Inf. Model. 47 (2007) 1045–1052.
[41] S.I. Gorelsky, AOMix program, revision 6.81, http://www.sg-chem.net/.
[42] S.I. Gorelsky, A.B.P. Lever, The electronic structure and spectra of [Ru(NH3)4(LL)]2+ (LL = bpy, bpz, bqdi) studied by density functional theory and INDO/S. charge transfer character of electronic transitions and their solvatochromism, Can. J. Anal. Sci. Spectrosc. 48 (2003) 93–105.
[43] G.U. Bublitz, S.G. Boxer, Effective polarity of frozen solvent glasses in the vicinity of dipolar solutes, J. Am. Chem. Soc. 120 (1998) 3988–3992.
[44] M.R. Feliz, F. Rodriguez-Nieto, G. Ruiz, E. Wolcan, Photophysical properties of Re(CO)3L+3 (L=monoazine) complexes: electronic delocalization effect in metal-to-ligand charge transfer excited states, J. Photochem. Photobiol. A 117 (1998) 185–192.
[45] M. Cattaneo, F. Fagalde, C.D. Borsarelli, N.E. Katz, Improvement of the dynamic range of pH sensing by using a luminescent tricarbonylpolypyridylrhenium(i) complex with three different protonation sites, Inorg. Chem. 48 (2009) 3012–3017.
[46] R. Liu, N. Dandu, Y. Li, S. Kilina, W. Sun, Synthesis, photophysics and reverse saturable absorption of bipyridyl platinum(ii) bis(arylfluorenylacetylide) complexes, Dalton Trans. 42 (2013) 4398–4409.
[47] D.L. Davies, F. Lelj, M.P. Lowe, K.S. Ryder, K. Singh, S. Singh, Pyridine imines as ligands in luminescent iridium complexes, Dalton Trans. 43 (2014) 4026–4039.

UNCORRECTED PROOF